Nanostructural characteristics, mechanical properties, and osteoblast response of spark plasma sintered hydroxyapatite

H. Li,[1]* K. A. Khor,[1] V. Chow,[1] P. Cheang[2]
[1]*School of Mechanical and Aerospace Engineering, Nanyang Technological University, 50 Nanyang Avenue, Singapore 639798*
[2]*School of Chemical and Biomedical Engineering, Nanyang Technological University, 50 Nanyang Avenue, Singapore 639798*

Received 3 April 2006; revised 16 June 2006; accepted 13 October 2006
Published online 1 February 2007 in Wiley InterScience (www.interscience.wiley.com). DOI: 10.1002/jbm.a.31143

Abstract: This study aimed to fabricate bulk nanostructured hydroxyapatite (HA) pellets with improved properties using spark plasma sintering (SPS) for orthopedic applications. Spray-dried nanostructured HA (nSD-HA) powders were consolidated using the rapid SPS processing. The SPS processed nSD-HA was characterized using Raman spectroscopy and field emission scanning electron microscopy (FESEM). Mechanical properties of the consolidates were also evaluated through indentation approach. The nanostructures (~80 nm in grain size) of the starting powders were successfully retained after the SPS processing operated at 950°C with <15 min holding time. The SPS consolidated nSD-HA showed promising mechanical properties, ~118 GPa for Young's modulus, and up to 2.22 MPa $m^{0.5}$ for fracture toughness. SPS holding time showed minor influence on the phases of the pellets. Furthermore, the spheroidized nanostructured HA retained the HA structure after the SPS consolidation. Preliminary cytotoxicity and cell attachment studies were also carried out using a human osteoblast cell line hFOB 1.19. Enhanced cell attachment and proliferation on the nanostructured pellets were revealed. The presence of the nanostructures accounts mainly for the enhanced mechanical properties and promoted proliferation of the osteoblast cells. This study suggests that the SPS technique is an appropriate process for fabrication of bulk nSD-HA from nanostructured powder. © 2007 Wiley Periodicals, Inc. J Biomed Mater Res 82A: 296–303, 2007

Key words: hydroxyapatite; spark plasma sintering; nanostructures; Young's modulus; fracture toughness; osteoblast cell

INTRODUCTION

Hydroxyapatite (HA) is an important biomaterial for hard tissue replacement owing to its similarity in chemistry to bone. Generally, since bulk HA is poor in mechanical properties, HA is used as biocompatible coating deposited on metallic implant, e.g., Ti6Al4V, through thermal spraying.[1–3] The HA-coated implants have shown promising effect on enhancing bone apposition and functional life after implantation.[4–6] However, the coating deposition processes incorporate an extra interface between the coating and substrate. Failure of the HA-coated implants took place mostly at the coating/substrate interface[7,8] because the interface is the weakest zone.[9] This in turn results in poor long-term stability of the HA-coated implants. In addition, for hard tissue replacement, there is, in many cases, requirement of the implants with small sizes. Study on fabrication of bulk HA is therefore essentially important. Generally utilized sintering process involves high temperature, e.g., 1300°C, and long sintering time, e.g., 1 h. These would introduce considerable HA phase transformation to other phases,[10,11] such as tricalcium phosphate (TCP), etc. Even though addition of other additives into HA is capable of improving the properties,[12] the process deteriorates the bioactivity.[13] Spark plasma sintering (SPS) is a rapid sintering process which is able to sinter ceramic powders quickly to their full density at a relatively lower temperature than the conventional sintering method.[14,15] The SPS features a very high thermal efficiency because of the direct heating of the sintering graphite mold and stacked powder materials by the large spark pulse current. These features probably enable SPS to be competitive in small HA

**Present address:* Biology Department, 50 Bell Avenue, Brookhaven National Laboratory, Upton, NY 11973, USA
Correspondence to: H. Li; e-mail: hli1@bnl.gov

implant fabrication with improved properties and less HA decomposition. Moreover, extensive studies revealed that the long-term performance and functional service duration of the HA-coated implants are influenced significantly by the microstructure of the coatings.[16,17] In recent years, nanostructured materials attracted intense interest due to their enhanced mechanical properties.[18,19] Previous *in vitro* study has also reported that nanosized ceramics are capable of enhancing osteoblast adhesion on them.[20] However, the challenge so far is how to avoid effectively the grain growth of the nanosized grains during the processing, since the nanostructures always encounter grain growth during high temperature sintering.[21–23] The rapid SPS processing provides the possibility of retaining the nanostructures from starting powders. The present study employed SPS for consolidating nanostructured HA (nSD-HA) and aimed to reveal the nanostructural features of the pellets. It was also to clarify the effect of the nanostructures on mechanical performances and biocompatibility of the SPS pellets.

EXPERIMENTAL

Starting powder

Spray-dried nSD-HA powders synthesized in-house via the wet chemical method were utilized for the SPS consolidation. These powders were heat-treated at 950°C for 1.5 h and X-ray diffraction (XRD) detections were performed to ensure their major component as stoichiometric HA. 950°C was found to be the critical annealing temperature for achieving stable HA structure. The agglomerated powder particles were composed of nanostructures (with rod-like grains: <230 nm in length and <70 nm in diameter) [Fig. 1(a,b)]. The powders with different particle size ranges, as determined by a laser particle size analyzer (analysette 22 NanoTec, FRITSCH, Germany), were utilized for the SPS consolidation, <20 μm, −45 + 20 μm, −75 + 45 μm, and −125 + 75 μm.

SPS parameters

The SPS system used was the Sumitomo Coal Mining (SCM) SPS system DR SINTER Model 1050. In this project, the SPS temperature was fixed for all the samples at 950°C. The temperature was detected by an infrared camera directly from the sample during the consolidation. The current (~500–1500 A) and voltage (~5–15 V) of the SPS system were controlled by the temperature during the sintering. Our previous systematic studies have shown that 950°C is the most suitable temperature for consolidating HA with minimal HA decomposition and at the same time high density can be accomplished. The only parameter that was varied was the SPS processing time, 3, 5, 10, 15, and 20 min. The SPS heating and cooling rate was 100°C/min. An initial low pressure of 4.5 Pa in the whole working chamber was applied and during SPS densification of the nSD-HA, the pressure level was maintained at 30 MPa.

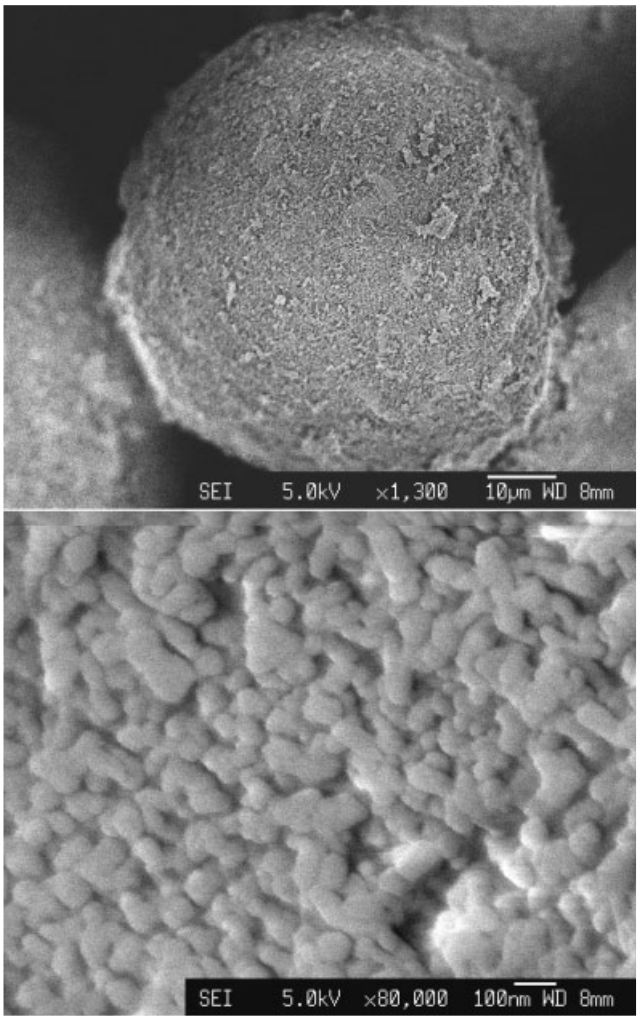

Figure 1. Morphology of the nSD-HA particles showing the nanostructures, (a) single particle and (b) closer examination showing agglomerated nanostructures.

Characterization methods

Raman scattering analyses were performed using a Renishaw Raman Imaging Microscope WiRE spectroscopy equipped with 50 mW Class 3B helium–neon laser (λ = 632.816 nm). The morphological features of the SPS pellets were observed by field emission scanning electron microscopy (FESEM, JEOL JSM-6340F). Phase composition of the samples was analyzed by means of XRD (MPD 1880, Philips, The Netherlands). The operating conditions were 40 kV and 30 mA by using Cu K_α radiation. The goniometer was set at a scan rate of 0.02°/s over a 2θ range of 20°–80°. Fourier transform infrared spectroscopy (FTIR, PerkinElmer system 2000) analysis was also conducted. The infrared spectrum with a resolution of 4 cm^{-1} and the scan number of 8 were adopted with a spectral region from 400 to 4000 cm^{-1}. Young's modulus of the SPS HA

pellets was determined through indentation test using a Vickers microindentation equipment (CSEM® MHT, Switzerland). The maximum load was 1 N with the loading rate of 1 N/min and the pause was 10 s. The unloading rate was 1 N/min. Fracture toughness was also measured through the indentation approach. The determination of the fracture toughness K_{Ic} has been described in detail in another article.[24] A Vickers load, 0.5 N, was applied on the polished pellets with a load application time of 15 s. A total of 10 points were collected for each type of the samples. The experiment was conducted on HMV-2000 Shimadzu microhardness tester.

Cell culture

In vitro culturing of osteoblast cells was conducted using the hFOB 1.19 cell line. This cell line was established by transfection of limb tissue obtained from a spontaneous miscarriage. Cells were cultured in Dulbecco's modified eagle medium containing 10% fetal bovine serum and 0.5% antibiotics in an atmosphere of 100% humidity and 5% CO_2 at 37°C. In this study, the cells were plated at 5×10^4 cells/mL in 24-well culture plates (with 1 mL media contained in each well). Proliferation of the cells cultured on the sterilized HA pellets (1 cm in diameter) after 2, 4, and 6 days was analyzed using the methyl thiazole tetrazodium (MTT) assay. The cells cultured in petri-dish without the nSD-HA samples were treated as control. The plates were read using 490 nm wavelength on a microplate reader machine (Benchmark Plus, Bio-Rad Laboratories). For each type of the pellets, five samples were tested to get an average value and each sample was read for three times.

RESULTS AND DISCUSSION

Raman spectra taken from the polished surface of the pellets (Fig. 2) indicate that the starting powder size has minor influence on the chemistry of the samples as the SPS holding duration is short, 5 min [Fig. 2(a)]. However, there exhibits obvious effect of starting particle sizes on the structure of the samples as the SPS time is longer, 15 min [Fig. 2(b)]. On the curves, the peaks at ~450 and 593 cm^{-1} refer to O—P—O bending modes (ν_2) of the PO_4 group in HA, the peak at ~964 cm^{-1} is assigned to P—O stretching mode (ν_1) of the PO_4 group in HA, the peaks at ~1051 and ~1096 cm^{-1} refer to P—O stretching mode (ν_3) of the PO_4 group. The peak at ~3574 cm^{-1} refers to O—H stretching of OH^- in HA. As the SPS holding time was 15 min, finer HA particles result in the structures with more HA characteristics [with the appearance of stronger OH^- peak at 3570 cm^{-1} and PO_4^{3-} peak for HA at ~450 and 610 cm^{-1} in Fig. 2(b)]. The peak at ~1620 cm^{-1} refers to H—O—H bending of H_2O. To further reveal the influence of the SPS holding time on the

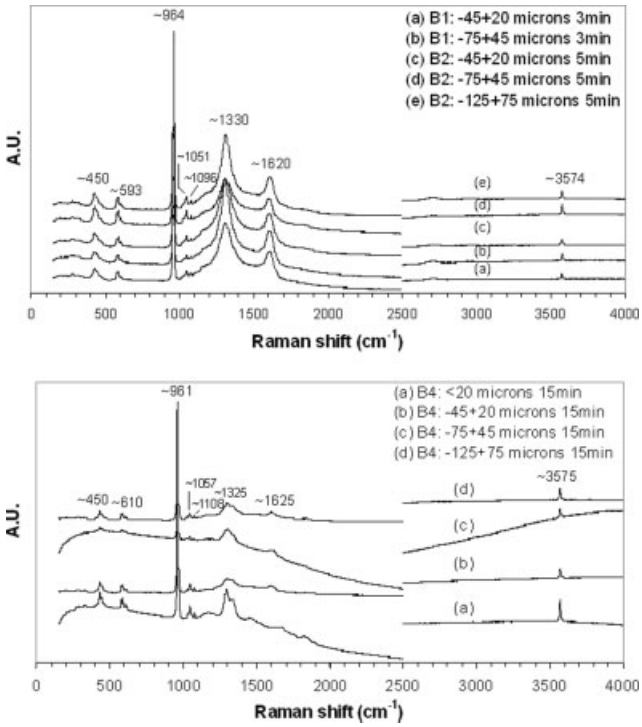

Figure 2. Raman spectra of the SPS consolidated nSD-HA showing the influence of the particle sizes and SPS holding time on the chemical structures of the pellets (to obtain refined curves, each sample was detected for two times, one was from 100 to 2500 cm^{-1} and the other one was from 2500 to 4000 cm^{-1}).

microstructure of the nSD-HA discs, the HA powders with a particle size range of −45 to +25 μm were typically systematically studied (Fig. 3). It is noted that the increase in peak intensity, which refers to HA content, increases with the increase of sintering time. It shows the evidence that for these powders, with increase of sintering time at 950°C, characteristics of crystalline HA become more evident. This on the other hand further indicates that the longer SPS consolidation time did not induce detectable HA decomposition. It has been found that the SPS processing triggered preferred phase orientation of TCP in SPS HA coatings.[25] The effect brought about by the longer holding time that more HA characteristics were detected might be attributed to the reorganization of HA structure.

It has been realized that the starting nSD-HA powders have typical porous structures. The structure could be improved through spheroidization processing attained by plasma spraying. In this study, the nSD-HA powders with the particle size range of <20 μm were spheroidized followed by SPS consolidation. Table I tabulates the spray parameters used for the spheroidization. Compared to the starting nSD-HA [Fig. 1(a)], the spheroidized HA (nS-HA) particles show an ideal spherical shape with dense structure and reorganized nanostructures [Fig. 4(a)].

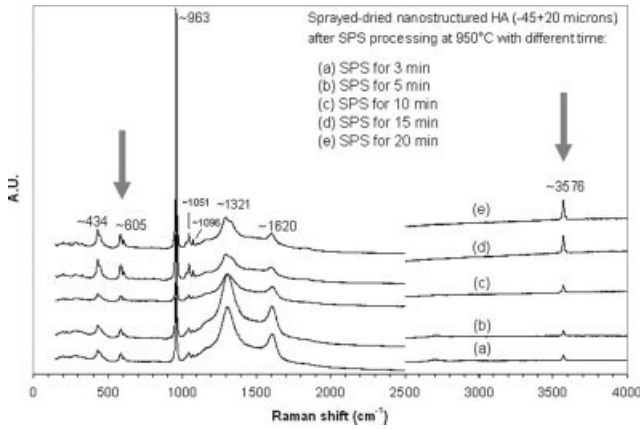

Figure 3. Raman spectra of the SPS consolidated nSD-HA pellets ($-45 + 20$ μm) processed with different holding time.

Close examination of the nanostructures exhibited at the particle surface [Fig. 4(b)] suggests predominate presence of the nanosized grains with the size of $\sim$50 nm (with a range of 40–100 nm). It has been found that 950°C was the optimum SPS temperature for the nS-HA powders since too low or too high temperatures triggered either poor consolidation or obvious HA decomposition to TCP, CaO, etc. XRD characterization suggests minor phase changes (Fig. 5) by the spheroidization process using plasma spraying operated at 2 kW. Furthermore, no phase changes were detected for the nS-HA after the SPS consolidation at 950°C for 5 min. However, Raman spectra reveal chemical structure differences between the nSD-HA and nS-HA pellets (Fig. 6). The peak referring to OH^- in HA (3575 cm^{-1}) disappeared for the nS-HA discs. This may suggest possible HA crystal structure changes, which needs to be further clarified. Furthermore, the nanostructures in the nS-HA powders were effectively retained after the SPS processing (Fig. 7). Grain growth is revealed at some areas, which might be triggered by the discharging between the particles during the SPS processing. The SPS process applied an on–off pulse voltage and current from a special pulse generator to powder particles. The discharges were then effectively activated between particles of powder at the initial stage of the pulse energizing for sintering. Those particles' interfaces encounter the highest temperatures due to

TABLE I
Plasma Spray Parameters for Spheroidization of nSD-HA Powders

Net energy	2 kW
Primary gas (Ar)	28.3 L/min
Auxiliary gas (He)	18.87 L/m
Carrier gas (Ar)	9.43 L/m
Powder feed rate	10 g/min
Spray angle	85°
Spray distance	250 mm

Spray angle and spray distance were taken with respect to the surface of distilled water. After drying of the spheroidized HA powders in 80°C oven, they were sieved for further SPS processing.

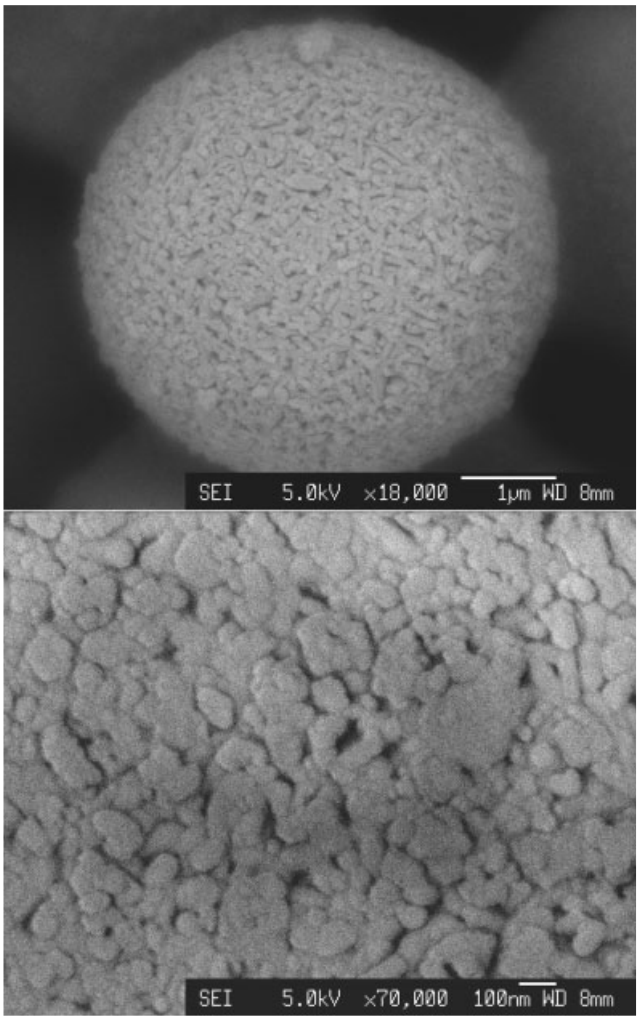

Figure 4. Typical topographical FESEM photos of the S-HA particles showing a spherical shape (a) and reorganized nanostructures (b).

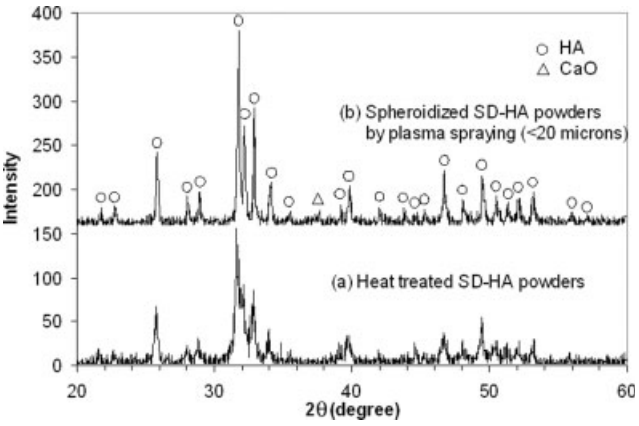

Figure 5. XRD patterns of nS-HA and nSD-HA powders.

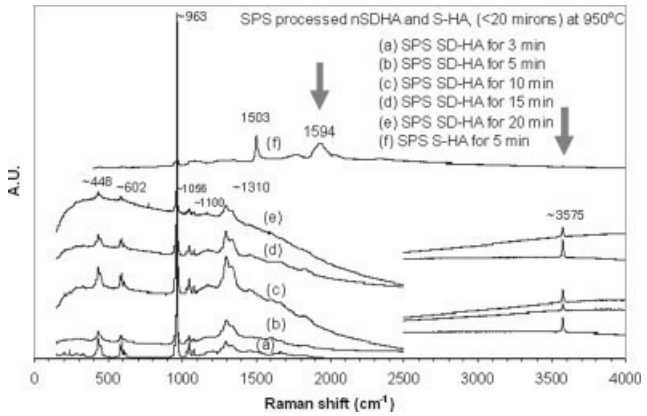

Figure 6. Raman spectra of the SPS consolidated nSD-HA (<20 μm) and nS-HA (<20 μm) pellets.

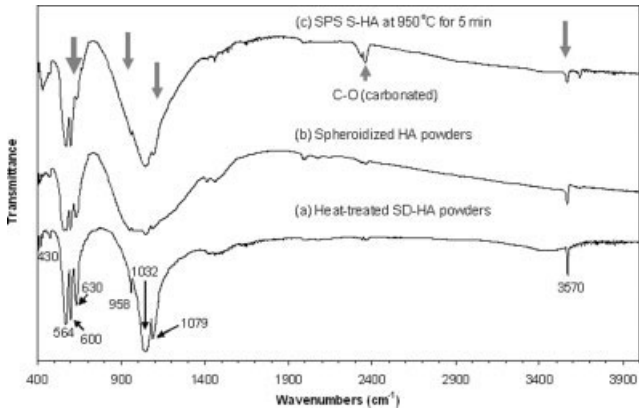

Figure 8. FTIR curve of the SPS consolidated nS-HA pellets with comparison to those of starting nSD-HA and nS-HA powders.

the spark generation. The comparison between nS-HA and nSD-HA pellets suggests that the 950°C sintering for 5 min has already resulted in structure changes of nS-HA, which are yet unclear so far and undetectable by XRD. A carbonated structure in the nS-HA discs is also revealed, which is suggested by the appearance of the peak labeled at ~1594 cm^{-1} (Fig. 6). Moreover, FTIR results further confirm the loss of OH^- during the high temperature SPS processing of the nS-HA (Fig. 8). On the curves, the peaks at 436 and 455 cm^{-1} are assigned to O—P—O bending mode (ν_2) of the PO_4^{3-} group in HA. And the peaks labeled at 591, 595, and 611 cm^{-1} refer to O—P—O bending mode (ν_4) of the PO_4^{3-} group in HA. 965 cm^{-1} peak is corresponding to P—O bond symmetric stretching mode (ν_1) of the tetrahedral PO_4^{3-} group in HA. The peaks at 1038, 1051, and 1080 cm^{-1} are for P—O bond asymmetric stretching mode (ν_3) of the PO_4^{3-} group in HA. It is further confirmed that the SPS nS-HA showed carbonated structure (the peak at 1503 cm^{-1}, C—O stretching, Fig. 8), which has been proven to possess higher osteoconductive properties and earlier bioresorption than HA.[26] The strong peak at 3577 cm^{-1}, which represents O—H stretching of OH^- in HA, shows consistence with the result suggested by the Raman spectra that most of HA is retained during the SPS consolidation.

A relative density of 96.5–99.7% with inhomogeneous structure of the nSD-HA pellets has been achieved by the SPS processing (Fig. 9). The values were determined by the Archimedes method with assuming the theoretical density of HA as 3.16 g/cm^3. The increase in SPS holding time, from 3 to 20 min, results in an increase in the density. The highest density is observed for the pellet made from the powders with the size <20 μm. This is not surprising since finer powders can be better consolidated. Furthermore, the mechanical property evaluation shows that the SPS consolidated nSD-HA discs have a Young's modulus of up to 118 GPa and fracture toughness with a range from 1.20 to 2.22 MPa $m^{0.5}$ (Fig. 10). The SPS nS-HA pellets with 5 min

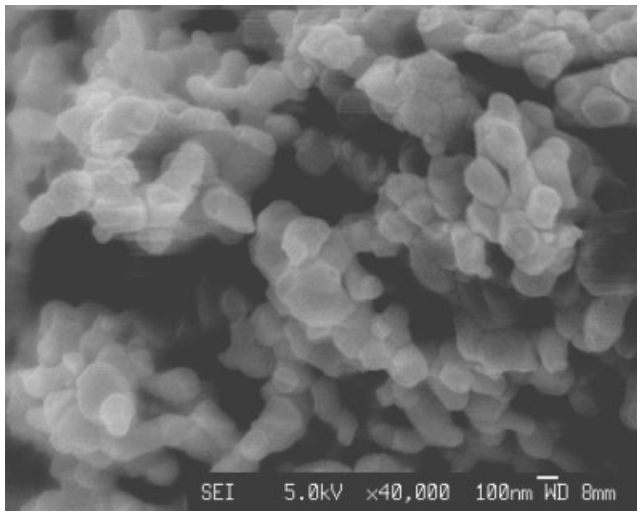

Figure 7. Fractured nS-HA pellets showing retained nanosized HA grains.

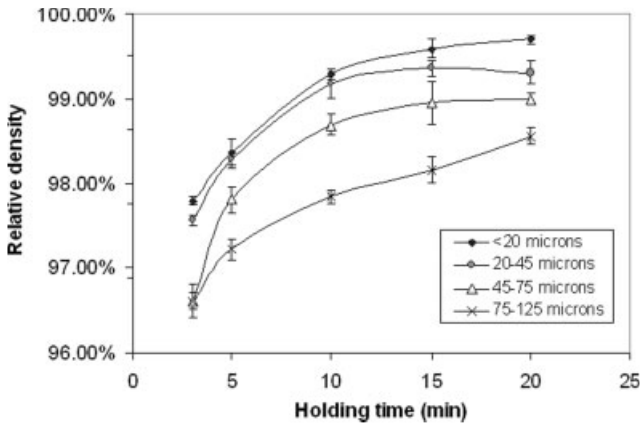

Figure 9. Relative density of the SPS consolidated nSD-HA pellets (the error bar means standard deviation).

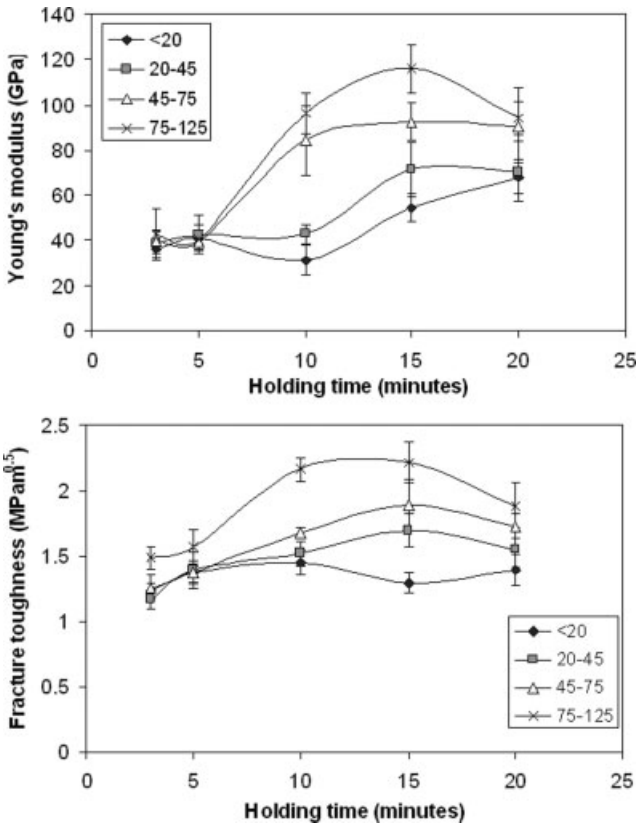

Figure 10. Young's modulus (a) and fracture toughness K_{Ic} (b) of the SPS consolidated nSD-HA.

holding time also showed competitive values, 45 GPa of Young's modulus and 1.41 MPa $m^{0.5}$ of fracture toughness. The fracture toughness and Young Modulus tend to be higher with longer holding time (till 15 min) and coarser particle sizes. The Young's moduli obtained are higher than those reported values for HA samples, 16.2 GPa by plasma spray,[27] 21 GPa by HVOF,[28] and 108 GPa by traditional sintering at 1300°C.[29] The high Young's modulus obtained in this study is consistent with the value of theoretical dense HA, which has been discussed by Lopes et al.[29] The SPS processing temperature, 950°C, is still relatively lower than the starting point of HA transformation (~1000°C[30]). Consequently, HA is successfully retained without evidence of thermal decomposition. Traditional sintering technique, which usually employed higher temperature, e.g., 1200°C, often resulted in undesirable HA transformation to other phases, such as TCP, etc.[10] The predominate presence of HA may also contribute to the enhanced mechanical properties.

Furthermore, even though the temperatures at the contact areas among the HA particles might be higher due to the possible discharging during the SPS processing, it is found that most of the nanostructures can be effectively retained owing to the short heating period of time. However, it is noted that the size of the nanosized grains alters depending on the sintering duration (Fig. 11). For the SPS nSD-HA (with the particle sizes of −45 + 20 μm),

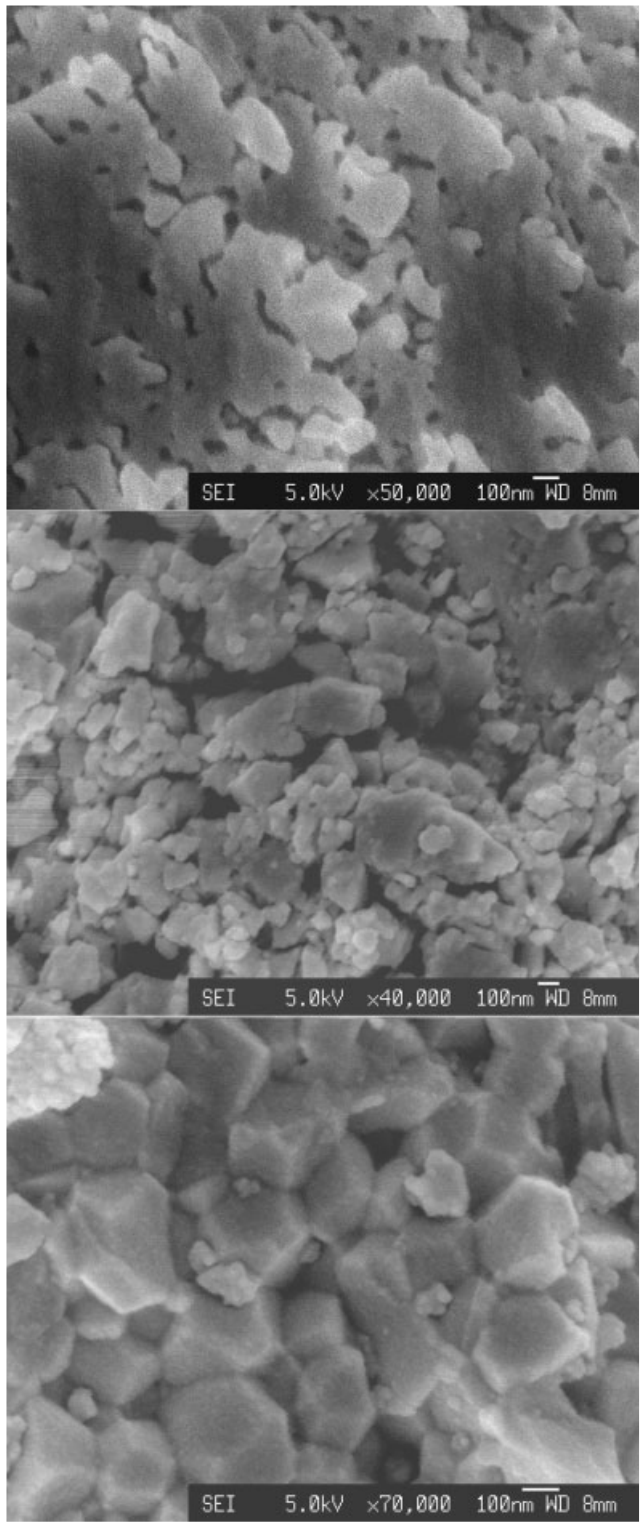

Figure 11. Typical morphological features of the SPS consolidated nSD-HA pellets (made from −45 to +20 μm powders) showing increased grain sizes from (a) ~80 nm (5 min holding time), (b) ~80 nm (15 min holding time), to (c) ~210 nm (20 min holding time).

the grain sizes are ~80 nm for the pellets consolidated for 5 min, ~80 nm (with some enlarged grains) for the pellets processed for 15 min, and ~210 nm for the pellets processed for 20 min. It is obvious that the nanostructures can only be retained as far as the SPS processing time is less than 15 min. These results favorably account for the high Young's modulus and fracture toughness values shown in Figure 10. These are consistent with other researchers' results that nanostructured ceramics possess superior mechanical properties compared to traditional ceramics.[18,19,31] Increased density (Fig. 9) also contributes to the enhanced mechanical properties, however, as the SPS holding time is 20 min, the significantly enlarged grains deteriorate such effects. This nevertheless claims the significant influence of the nanostructures on the mechanical properties of the samples. Some previous studies also reported similar findings that the nanostructures may account for enhanced mechanical properties.[18,19] Furthermore, it is evident that the nanorods present in the starting powders [Fig. 1(b)] retained their size as the SPS holding time is less than 15 min. The present SPS processing provides rapid consolidation which can effectively minimize the surface diffusion among the nanostructured particles. Generally, during the later stage of the sintering, the model $G^n = G_0^n + Kt\ \exp\left(-\frac{Q}{\kappa T}\right)^{21}$ prevails, where G is the grain size, G_0 is the initial grain size, n is typically 3, K is a rate constant, t is the time, T is the absolute temperature, κ is the Boltzmann's constant, and Q is the activation energy for grain growth. Obviously, the shorter consolidation time t provided by SPS than traditional sintering contributes to the retained nanosized grains in the HA discs. However, for the current SPS processing, there seems to be a threshold time up to which point the nanosized grains start to grow rapidly. In addition, the polished cross-sections of the typical SPS processed nSD-HA pellets show the nanosized pores ranging from ~13 to ~65 nm [Fig. 11(a)]. However, the effect of the nanosized pores in the SPS pellets on their mechanical properties is unclear yet.

The *in vitro* behavior of the SPS nSD-HA was preliminarily studied through MTT assay. The samples with the SPS holding time 5 min were typically investigated *in vitro*. Result shows that the SPS consolidated HA pellets enhance attachment and proliferation of the cells (Fig. 12), which in turn suggests the marked biocompatibility of the pellets. The highest value achieved by the SPS nS-HA evidences the ability of the carbonated structure to enhance the biocompatibility. It has been discussed previously that the nanostructures were successfully retained after the 5 min SPS consolidation. The nanostructures in the SPS pellets may provide dense surfaces, which in turn decreases the surface energy, while the reduced surface energy promotes initial attachment and spreading of the cells and improves their attachment.[32] This could explain the high MTT values exhibited by the nSD-HA pellets after the 2 days incubation. In addition, the nSD-HA discs can supply more particle/grain boundaries, which were found to be the sites where the osteoblast adhesion occurred preferentially.[33] However, after the incubation with different periods of time, 2, 4, and 6 days, no significant difference was revealed among the samples. It seems that the slight differences in phases (as stated by the structure analyses) possess less effect than the nanostructures on the proliferation of the osteoblast cells. Further refined research about the effect of the nanostructures on their osteoblast behavior is to be conducted.

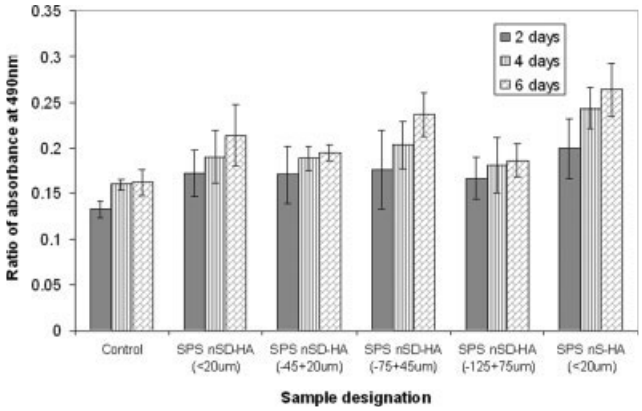

Figure 12. MTT results of the SPS nSD-HA and nS-HA pellets showing the marked biocompatibility of the pellets and enhancing effect of the carbonated structure in SPS nS-HA on proliferation of the osteoblast cells.

CONCLUSIONS

The present study suggests that the SPS consolidation processing is capable of fabricating bulk nSD-HA discs without obvious loss of HA and favorable mechanical properties were achieved, 118 GPa Young's modulus and 2.22 MPa $m^{0.5}$ fracture toughness. SPS consolidated nSD-HA at 950°C exhibited a dense structure (with up to 99.7% relative density) and minor phase transformation as the SPS holding time is <20 min. The nanostructures (~80 nm) in the starting nSD-HA powders are successfully retained after the 950°C SPS consolidation as the SPS holding time is less than 15 min. The particle size of the starting powders does not show obvious influence on the microstructures of the SPS pellets. Compared to SPS nSD-HA, the SPS consolidated nS-HA showed a structure with carbonate substitution, which enhanced the proliferation of the osteoblast cells. The nanostructures in the nSD-HA/nS-HA pellets significantly contribute to enhanced

mechanical properties. The preliminary *in vitro* experiment showed that the slight differences in phases (as stated by the structure analyses) possess less effect than the nanostructures on the proliferation of the osteoblast cells. The optimal SPS treating parameters were found to be using starting powders of <20 μm and a holding time of 15 min at $\sim 950^{\circ}$C.

References

1. Klein CPAT, Patka P, Wolke JGC, de Blieck-Hogervorst JMA, de Groot K. Long-term in vivo study of plasma-sprayed coatings on titanium alloys of tetracalcium phosphate, hydroxyapatite and α-tricalcium phosphate. Biomaterials 1994;15:146–150.
2. Li H, Ng BS, Khor KA, Cheang P, Clyne TW. Raman spectroscopy determination of phases within thermal sprayed hydroxyapatite splats and subsequent in vitro dissolution examination. Acta Mater 2004;52:445–453.
3. Sun L, Berndt CC, Grey CP. Phase, structural and microstructural investigations of plasma sprayed hydroxyapatite coatings. Mater Sci Eng A 2003;360:70–84.
4. Pendegrass CJ, Oddy MJ, Cannon SR, Briggs T, Goodship AE, Blunn GW. A histomorphological study of tendon reconstruction to a hydroxyapatite-coated implant: Regeneration of a neo-enthesis in vivo. J Orthop Res 2004;22:1316–1324.
5. Hardy DCR, Frayssinet P, Delince PE. Osteointegration of hydroxyapatite-coated stems of femoral prostheses. Eur J Orthop Surg Traumatol 1999;9:75–81.
6. Yoshikawa T, Ohgushi H, Tamai S. Immediate bone forming capability of prefabricated osteogenic hydroxyapatite. J Biomed Mater Res 1996;32:481–492.
7. Krauser JT, Berthold P. A scanning electron microscopy study of failed root from dental implant. J Dental Res 1991;70:274–281.
8. Inadome T, Hayashi K, Nakashima Y, Tsumura H, Sugioka Y. Comparison of bone–implant interface shear strength of hydroxyapatite-coated and alumina-coated implants. J Biomed Mater Res 1995;29:19–24.
9. Shaw LL, Barber B, Jordan EH, Gell M. Measurements of the interfacial fracture energy of thermal barrier coatings. Scripta Mater 1998;39:1427–1434.
10. Kothapalli C, Wei M, Vasiliev A, Shaw MT. Influence of temperature and concentration on the sintering behavior and mechanical properties of hydroxyapatite. Acta Mater 2004;52:5655–5663.
11. Anee TK, Ashok M, Palanichamy M, Kalkura SN. A novel technique to synthesize hydroxyapatite at low temperature. Mater Chem Phys 2003;80:725–730.
12. Kalita SJ, Bose S, Hosick HL, Bandyopadhyay A. CaO-P_2O_5-Na_2O-based sintering additives for hydroxyapatite (HAp) ceramics. Biomaterials 2004;25:2331–2339.
13. Jun YK, Kim WH, Kweon O, Hong S. The fabrication and biochemical evaluation of alumina reinforced calcium phosphate porous implants. Biomaterials 2003;24:3731–3739.
14. Johnson DL. Microwave and plasma sintering of ceramics. Ceram Int 1991;17:295–300.
15. Gao L, Wang HZ, Hong JS, Miyamoto H, Miyamoto K, Nishikawa Y, Torre SDDL. SiC-ZrO_2(3Y)-Al_2O_3 nanocomposites superfast densified by spark plasma sintering. Nanostruct Mater 1999;11:43–49.
16. Suominen E, Aho AJ, Vedel E, Kangasniemi I, Uusipaikka E, Yli-Urpo A. Subchondral bone and cartilage repair with bioactive glasses, hydroxyapatite, and hydroxyapatite-glass composite. J Biomed Mater Res 1996;32:543–551.
17. Szivek JA, Anderson PL, Dishongh TJ, de Young DW. Evaluation of factors affecting bonding rate of calcium phosphate ceramic coatings for in vivo strain gauge attachment. J Biomed Mater Res 1996;33:121–132.
18. Zhu YC, Yukimura K, Ding CX, Zhang PY. Tribological properties of nanostructured and conventional WC-Co coatings deposited by plasma spraying. Thin Solid Films 2001;388:277–282.
19. Berndt CC, editor. Thermal spray processing of nanoscale materials II—Extended abstracts. J Therm Spray Technol 2001;10:147–182.
20. Webster TJ, Siegel RW, Bizios R. Osteoblast adhesion on nanophase ceramics. Biomaterials 1999;20:1221–1227.
21. German RM. Sintering Theory and Practice. New York: Wiley; 1996.
22. Choi SY, Kang SL. Sintering kinetics by structural transition at grain boundaries in barium titanate. Acta Mater 2004;52: 2937–2943.
23. Zhou Y, Hirao K, Yamauchi Y, Kanzaki S. Densification and grain growth in pulse electric current sintering of alumina. J Eur Ceram Soc 2004;24:3465–3470.
24. Li H, Khor KA, Cheang P. Young's modulus and fracture toughness determination of HVOF sprayed bioceramic coatings. Surf Coat Technol 2002;155:21–32.
25. Yu LG, Khor KA, Li H, Cheang P. Effect of spark plasma sintering on the microstructure and in vitro behavior of plasma sprayed HA coatings. Biomaterials 2003;24:2695–2705.
26. Landi E, Celotti G, Logroscino G, Tampieri A. Carbonated hydroxyapatite as bone substitute. J Eur Ceram Soc 2003;23:2931–2937.
27. Yang YC, Chang E, Hwang BH, Lee SY. Biaxial residual stress states of plasma-sprayed hydroxyapatite coatings on titanium alloy substrate. Biomaterials 2000;21:1327–1337.
28. Li H, Khor KA, Cheang P. Properties of heat-treated calcium phosphate coatings deposited by high-velocity oxy-fuel (HVOF) spray. Biomaterials 2002;23:2105–2112.
29. Lopes MA, Silva RF, Monteiro FJ, Santos JD. Microstructural dependence of Young's and shear moduli of P_2O_5 glass reinforced hydroxyapatite for biomedical applications. Biomaterials 2000;21:749–754.
30. Hideki A. Medical Applications of Hydroxyapatite. Tokyo, St. Louis: Ishiyaku EuroAmerica; 1994.
31. Gell M, Jordan EH, Sohn YH, Goberman D, Shaw L, Xiao TD. Development and implementation of plasma sprayed nanostructured ceramic coatings. Surf Coat Technol 2001;146/147: 48–54.
32. Redey SA, Nardin M, Bernache-Assolant D, Rey C, Delannoy P, Sedel L, Marie PJ. Behavior of human osteoblastic cells on stoichiometric hydroxyapatite and type A carbonate apatite: Role of surface energy. J Biomed Mater Res 2000;50:353–364.
33. Webster TJ, Ejiofor JU. Increased osteoblast adhesion on nanophase metals: Ti, Ti_6Al_4V, and CoCrMo. Biomaterials 2004;25: 4731–4739.